Fermi National Accelerator Laboratory

FERMILAB-Conf-78/46-EXP
7410.021

CHARGED CURRENT NEUTRINO AND ANTINEUTRINO CROSS SECTION RESULTS FROM THE CITFR EXPERIMENT*

B. C. Barish, J. F. Bartlett, A. Bodek, K. W. Brown
D. Buchholz, Y. K. Chu, F. Sciulli, E. Siskind,
and L. Stutte
California Institute of Technology
Pasadena, California 91125

and

H. E. Fisk, G. Krafczyk, and D. Nease
Fermi National Accelerator Laboratory
Batavia, Illinois 60510

and

O. Fackler
Rockefeller University
New York, New York 10021

June 1978

* Submitted to the 3rd International Conf. on New Results in High Energy Physics, Vanderbilt University, Nashville, March 6-8, 1978.

CHARGED CURRENT NEUTRINO AND ANTINEUTRINO CROSS SECTION RESULTS FROM THE CITFR EXPERIMENT

B. C. Barish, J. F. Bartlett,[a] A. Bodek,[b] K. W. Brown, D. Buchholz,[c] Y. K. Chu, F. Sciulli, E. Siskind, and L. Stutte[a]
California Institute of Technology
Pasadena, California 91125

and

H. E. Fisk, G. Krafczyk, and D. Nease
Fermi National Accelerator Laboratory
Batavia, Illinois 60510

and

O. Fackler
Rockefeller University
New York, New York 10021

INTRODUCTION

In the Summer and Fall of 1975 the CITFR group had a major data taking run to measure total charged current cross sections using a dichromatic beam. Much of the data from that run are published in the September 9 and December 19, 1977 Physical Review Letters. The objectives of that run included tests of Bjorken scaling in deep inelastic neutrino and antineutrino scattering. These tests are conventionally discussed in terms of the scaling variables x, y.[1] If the usual assumptions about scaling, V-A weak charged currents, isoscalar target, M_W large, etc., are made then:

$$\frac{d^2\sigma^{\nu,\bar{\nu}}}{dxdy} = \frac{G^2 M E_\nu}{\pi}\left\{(1-y)F_2^{\nu,\bar{\nu}}(x) + y^2/2\ 2xF_1^{\nu,\bar{\nu}}(x) \pm y(1-y/2)F_3^{\nu,\bar{\nu}}(x)\right\}, \quad (1)$$

$$Q^2 = 4\,E_\nu E_\mu \sin^2\theta_\mu/2,$$

$$x = Q^2/2ME_H,$$

$$y = E_H/E_\nu.$$

We report here only on the observed y dependence of the cross sections. Consequently the following integrals over the structure functions are defined:

$$f_1 \equiv \int xF_1(x)dx;\ f_2 \equiv \int F_2(x)dx;\ f_3 \equiv \int xF_3(x)dx. \quad (2)$$

The cross section expression then becomes:

$$\frac{d\sigma^{\nu,\bar{\nu}}}{dy} = \frac{G^2 M E_\nu}{\pi}\left\{(1-y)f_2 + (y^2/2)2f_1 \pm y(1-y/2)f_3\right\} \quad (3)$$

The thrust of our experimental effort was:

(1) To measure $\sigma_o \equiv \left.\frac{d\sigma}{dy}\right|_{y=0}$ and test the charge symmetry invariance of f_2 which implies $f_2^\nu = f_2^{\bar{\nu}}$.

(2) To check the linear rise of σ^{ν} , $\bar{\nu}$ with energy and the ratio $R_c = \sigma_{\bar{\nu}}/\sigma_{\nu}$. R_c was reported to increase from 0.4 at less than 12 GeV to 0.6 or 0.7 at 60 GeV by the HPWF group.[2]

(3) To measure < y > for the neutrino and antineutrino data. Some authors[3] have indicated a statistically significant increase in < y > for antineutrino interactions at 60 GeV which might indicate scaling violations or new particle production while other recently published data[4] shows no energy dependence in < y >.

(4) To check the energy independence of the integrated structure functions and the Callen-Gross relation ($2f_1 = f_2$).

(5) To look for possible evidence which might suggest the existence of new massive quarks which couple right-handedly to neutrinos.

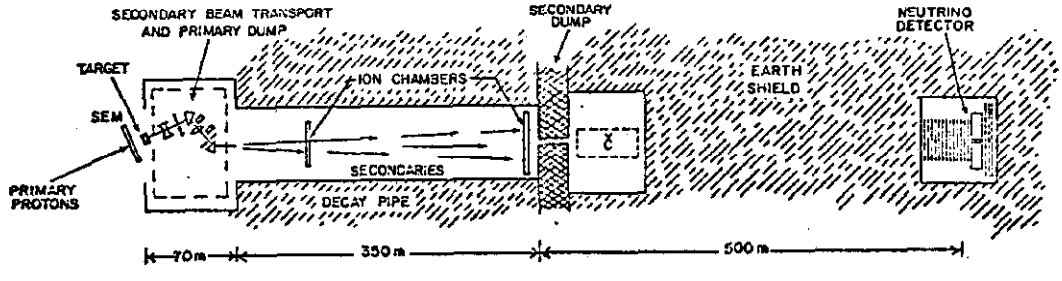

Fig. 1: E21 Dichromatic Beam and Apparatus.

BEAM AND APPARATUS

The dichromatic beam[5] and apparatus[6] which are shown in Fig. 1 have been discussed elsewhere. The 400 GeV proton beam is targeted on an aluminum block 1/2" W x 3/4" H x 12" L. The total intensity of secondary charged particles was measured with ionization chambers at two different points in the decay pipe (430 ft. and 1130 ft.). Both of these ion chambers were calibrated relative to each other and absolutely

to a foil irradiation and secondary emission monitor (SEM) by passing a 200 GeV primary proton beam through them simultaneously. The SEM was calibrated absolutely with single turn extracted beam from the Fermilab Main Ring and a toroid. The downstream ion chamber was separately calibrated in a low intensity, 10^6 ppp, 200 GeV proton beam where individual particles were counted. The agreement between the calibrations is 2%. During neutrino event data runs the two ion chambers tracked each other to better than 5% and disagreed to this extent because of beam containment within the ion chambers. Corrections up to 10% have been made for the specific ionization of the gas in the ion chambers for different species of particles (π, K, p) relative to the 200 GeV protons used for calibration.

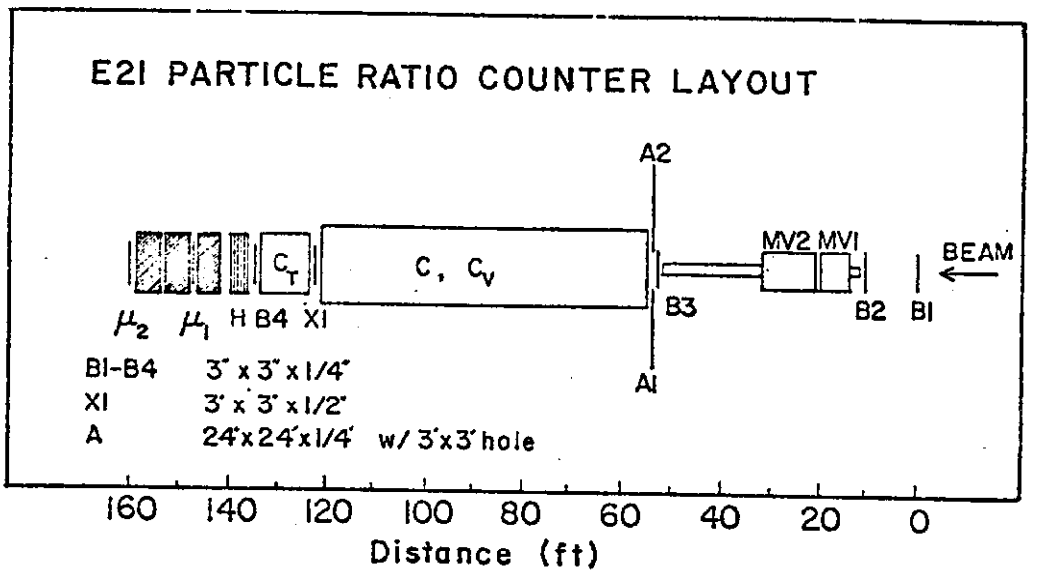

Fig. 2: Particle Ratio Measurement Apparatus.

To know the number of ν_K and ν_π at the apparatus, the $\pi^\pm$, $K^\pm$, p fractions of particles in the beam were measured. The counter arrangement is shown in Fig. 2. These counters were located immediately downstream of a steel dump at the end of the decay pipe. The secondary beam of reduced intensity (10^6 particles/pulse) entered the detectors through a 4" square hole in the dump. Both a sixty foot long differential counter and ten foot long threshold counter (set to count pions) were used in the measurement. The differential counter focussed 1.84 ± .016 mr light onto an iris of width 0.040". A pressure curve for -230

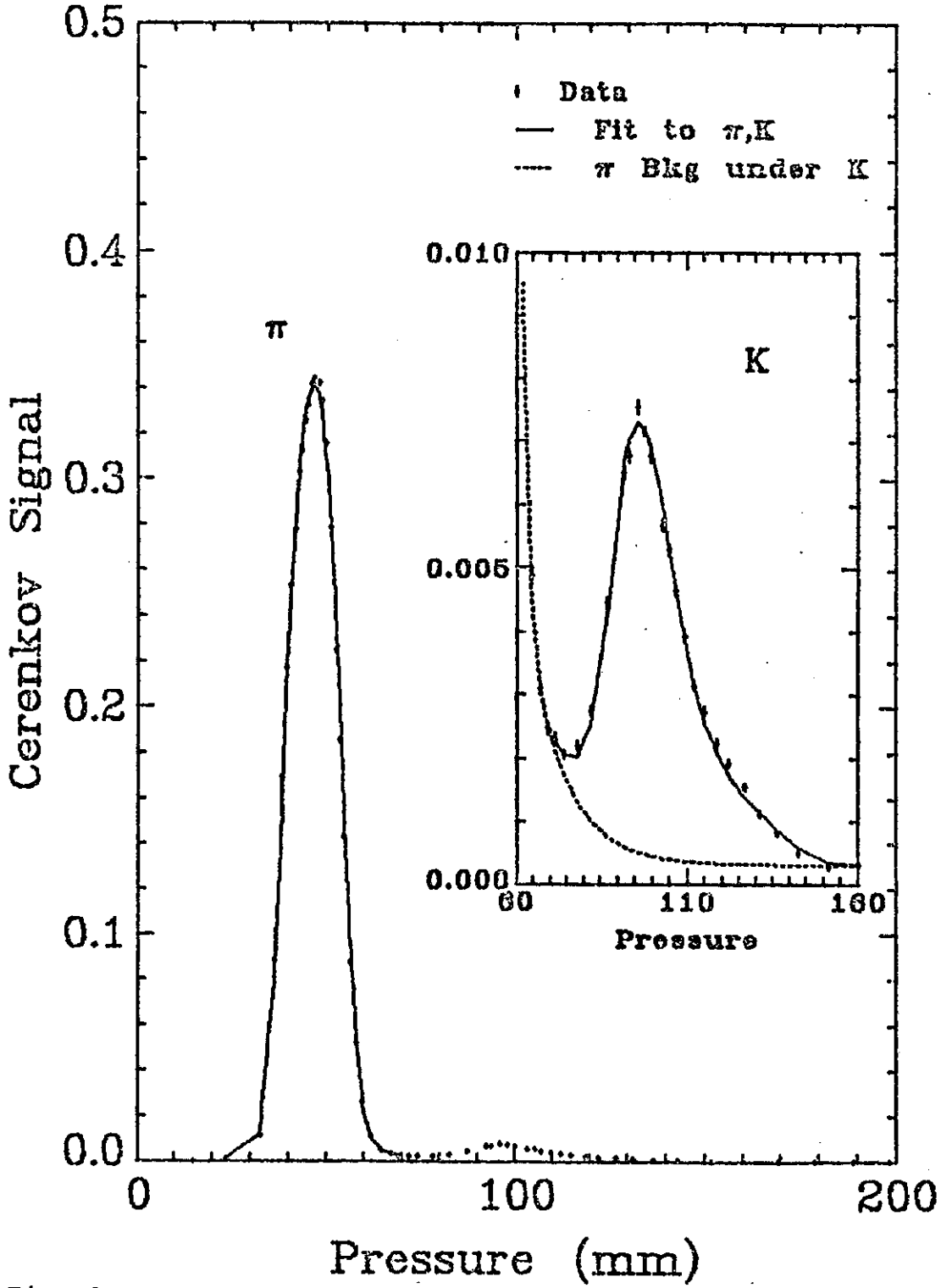

Fig. 3: Cerenkov pressure curve for the dichromatic beam tuned to -230 GeV. The inset shows the measured pion background under the K peak.

GeV is shown in Fig. 3. The inset shows the measured pion background under the K peak. Because the secondary beam was somewhat larger than the 4" hole at the end of the decay pipe, Cerenkov data were obtained by steering the beam, to sample different portions of the vertical and horizontal phase space. Table I and Fig. 4 show the particle fractions at the target for mean energies where neutrino event data were taken. The secondary particle production angles range from 0 to ±2 mr and the $\Delta p/p$ is ±16% (σ). The particle fractions are determined to ±(1-5)% for π's, ±(3-7)% for K's and ±(1-2)% for protons. This, combined with the ionization chamber data give overall ν_π and ν_K flux errors of ±(5 to 9)%.

Table I Particle Fractions vs. Mean Hadron Momentum

$< P_\pi >$	$< P_k >$, $< P_p >$	K/π	P/π
+122±19,	125±18, 131±19	0.103 ±0.004	0.989±0.018
+170±23,	173±23, 182±25	0.1295±0.005	3.076±0.065
+215±29,	218±28, 235±33	0.1618±0.013	8.029±0.406
-128±23,	-128±23	0.0567±0.0019	
-179±28,	-177±26	0.0472±0.0020	
-202±31,	-179±26	0.0458±0.0011	

EVENT DATA

A total of 18,000 ν and 12,000 $\bar{\nu}$ events were obtained with two triggers which are labeled muon and hadron.

MUON TRIGGERS

The muon trigger (MT) required a muon to penetrate the toroidal magnet (~2.4 m of steel and 1.5 m of target steel). In this case the measured quantities are E_h, E_μ, and θ_μ, with θ_μ restricted to angles less than 110 mr. These events are used to check the energy

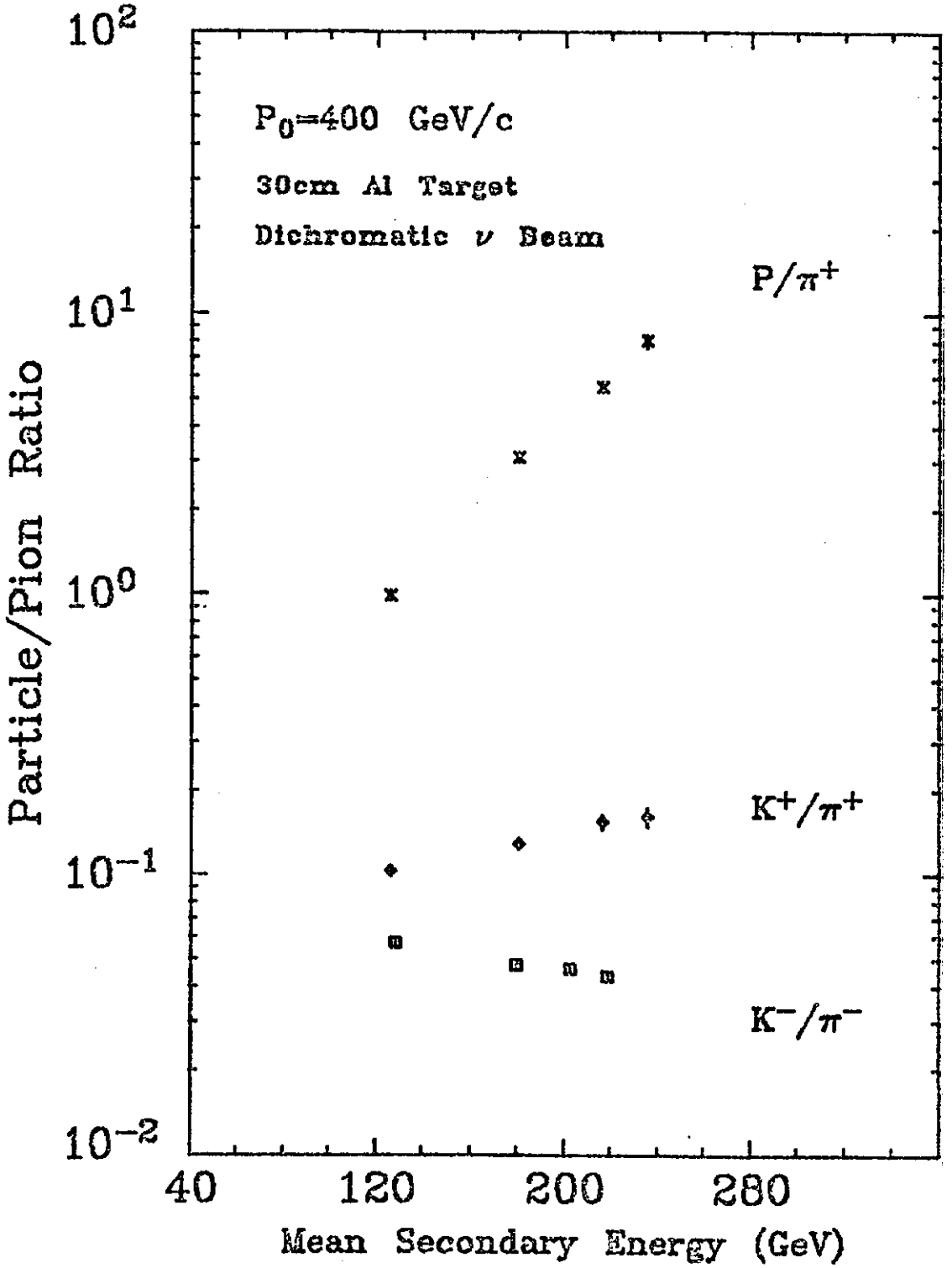

Fig. 4: Particle ratios vs. mean hadron energy.

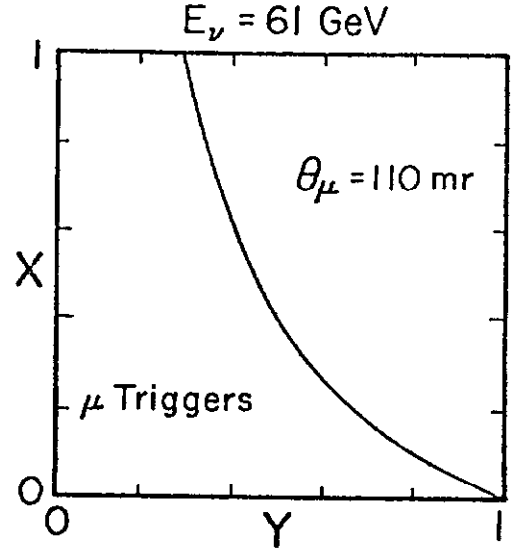

Figure 5a

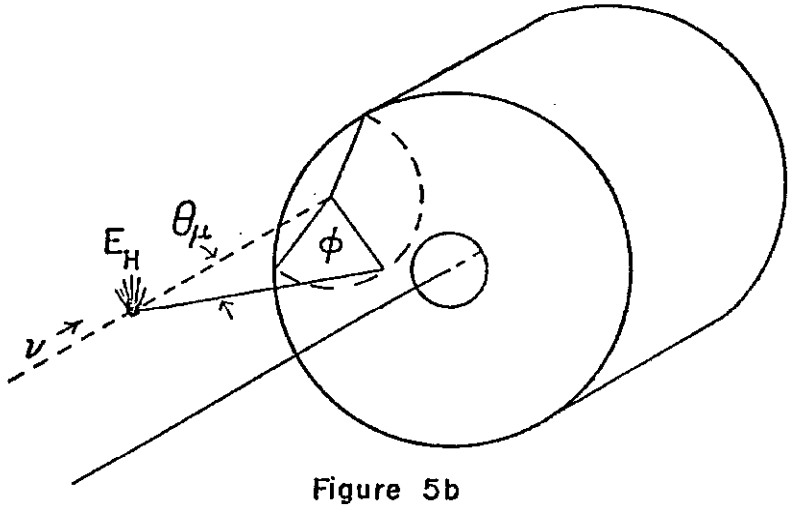

Figure 5b

Fig. 5: Muon trigger acceptance (5a) and geometrical event loss correction (5b). Muon triggers are accepted in the region to the left of the 110 mr curve in Fig. (5a).

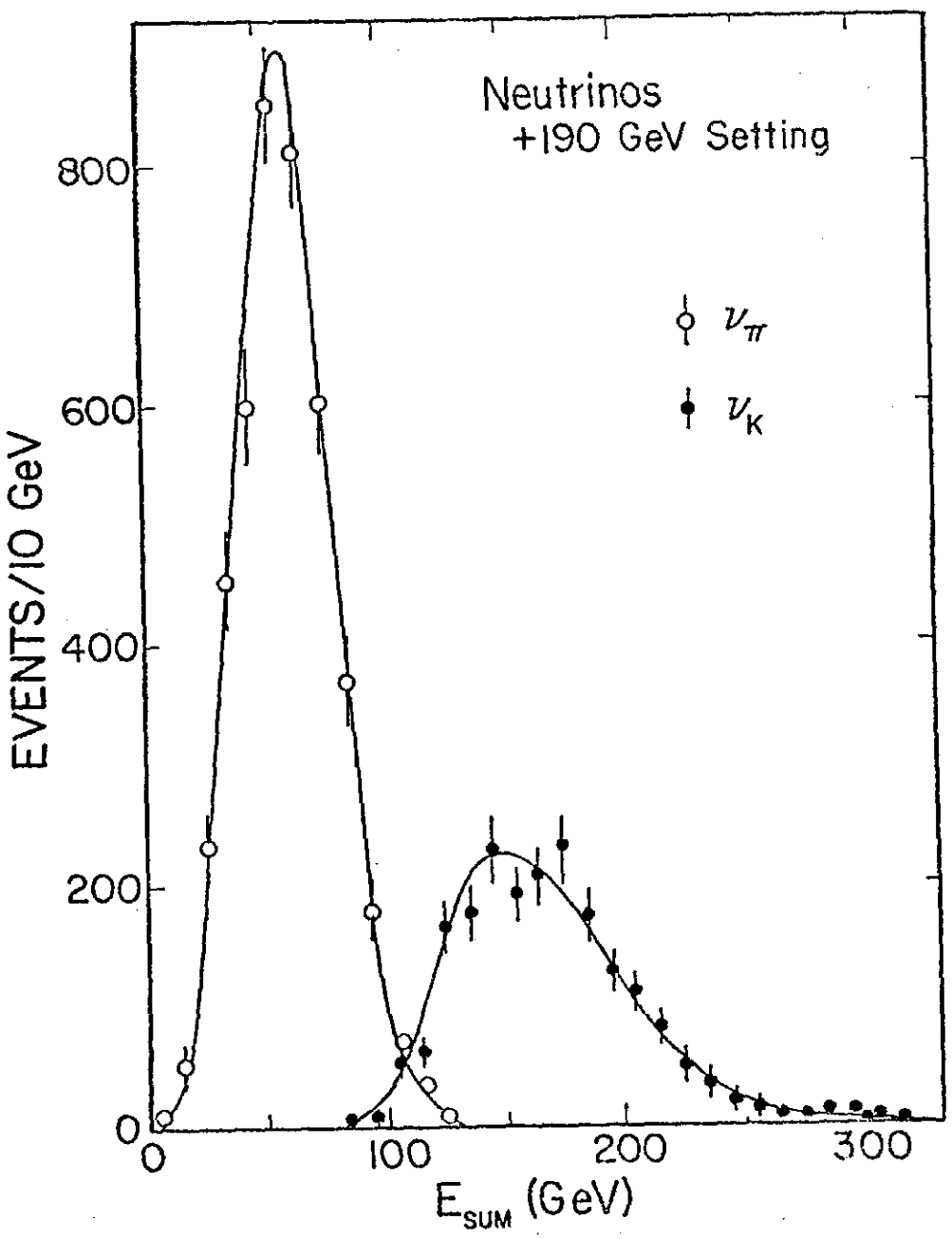

Fig. 6: Total energy distribution for muon trigger events (+190 GeV).

calibration of the calorimeter and muon spectrometer for both ν_K and ν_π at the six different beam momenta. The calibration agrees at all twelve energies to 4%.

In Fig. 5a the scaling variable MT acceptance is shown for a neutrino energy of 61 GeV. The y acceptance begins to be limited above y = 0.28. In the low y region geometrical event loss is fully corrected by the ϕ rotation defined in Fig. 5b. Since the total energy of the events is measured, the ν_K and ν_π data are separated. An example of this separation is shown in Fig. 6 for the +190 GeV data. The y = 0 cross sections are then obtained in the $y \leq 0.2$ region from:

$$\sigma_o = \left.\frac{d\sigma}{dy}\right|_{y=0} = \frac{CN}{FT\Delta y} \quad \text{where}$$

N is the number of events for $y \leq 0.2$, F is the flux, T is the number of target nucleons, Δy is 0.2 and C is a correction factor for the shape of the y distribution between y = 0 and y = 0.2. Figure 7 shows σ_o^{ν} and $\sigma_o^{\bar{\nu}}$ as a function of neutrino energy. If the form of σ_o/E_ν is assumed to be $a + b\,E_\nu$, then a best fit to the data of Fig. 7 yield (in units of 10^{-38} cm^2/GeV):

$$\sigma_o^{\nu}/E_\nu = (0.77\pm0.06)-(0.66\pm0.65)\times10^{-3}\,E_\nu \text{ and}$$

$$\sigma_o^{\bar{\nu}}/E_{\bar{\nu}} = (0.75\pm0.06)-(0.24\pm0.50)\times10^{-3}\,E_{\bar{\nu}}.$$

Clearly the data are consistent with a single value of σ_o/E_ν and the charge symmetry hypothesis: $\sigma_o^{\nu} = \sigma_o^{\bar{\nu}}$. The best combined fit gives $\sigma_o/E = (0.719 \pm 0.035) \times 10^{-38}$ cm^2/GeV which in terms of the integrated structure function is $\int F_2^{\nu n}(x)dx = 0.46 \pm 0.02$ at a mean Q^2 of about 5 GeV^2. This value agrees with the Gargamelle result of 0.49 ± 0.05 obtained at energies below 12 GeV.[7] The value of $\int F_2(x)\,dx$ obtained this way, from the low y cross section, is independent of the Callen-Gross assumption of spin 1/2 partons. The integral $F_2^{\nu N}(x)dx$ is consistent with the expected mean squared charge of the three quark model from

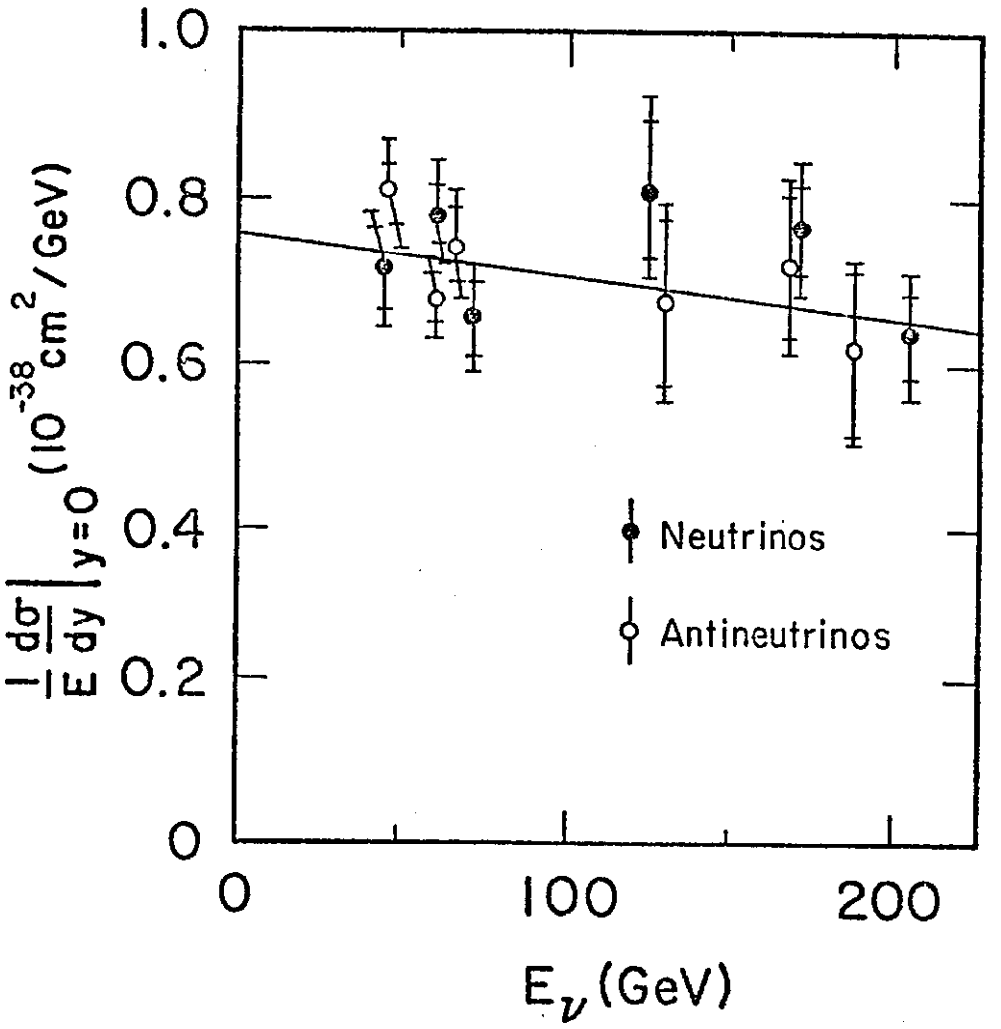

Fig. 7: Cross Sections at y=0 for the test of charge symmetry. The inner error bars are statistical while the outer limits include the systematics which are mainly due to the flux errors.

predictions which relate electron or muon-deuteron scattering and neutrino nucleon scattering:

$$\int F_2^{\nu N}(x)dx \leq 18/5 \int F_2^{\mu d}(x)dx,$$

where $\int F_2^{\mu d}(x)\,dx$ is measured to be 0.153 ± 0.005 for muons[8] and 0.147 ± .06 to 0.178 ± 0.04 for electrons.[9]

HADRON TRIGGERS

To measure total cross sections, neutrino data were also obtained with a hadron trigger. The hadron trigger required an average energy deposition in the calorimeter of at least 6 GeV. To be certain the event was a charged current neutrino interaction, a penetration requirement of 1.5 meters of steel (~9 absorption lengths) was imposed on the outgoing muon in the analysis. This condition implies muon angular acceptance out to 360 mr. The hadron trigger data were efficiency corrected by azimuthal weighting as were the muon trigger data.

Figure 8a shows the acceptance regions for both the muon and hadron triggers at a neutrino energy of 61 GeV ($< E_{\nu_\pi} >$ at 190 GeV). The substantial region of overlap for the two triggers allows a determination of efficiencies:

$$\epsilon_\mu = 97 \pm 1\% \text{ and}$$

$$\epsilon_H = 95 \pm 1\% \text{ for } E_H > 10 \text{ GeV}.$$

SEPARATION OF ν_π, ν_K EVENTS

In Fig. 8b a similar acceptance plot is shown for the mean ν_K energy, scaled by the mean energy ratio $< E_{\nu_K} > / < E_{\nu_\pi} >$. From a comparison of figures 8a and 8b it can be seen that all of the ν_K events, which have hadron energy in an E_H region ambiguous with ν_π data, are muon trigger events and are consequently identified as ν_K data from total energy. Events with

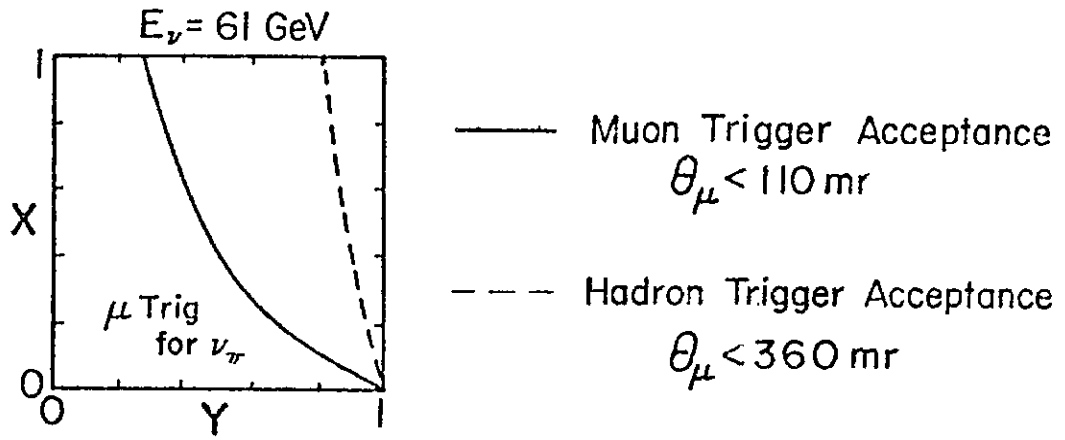

Fig. 8a

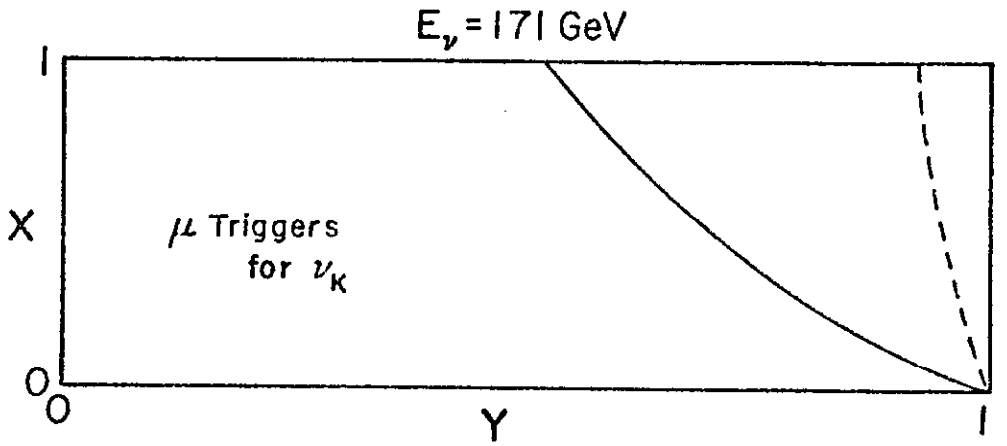

Fig. 8b

Fig. 8: Muon and hadron trigger acceptances for neutrinos of energy 61 and 171 GeV.

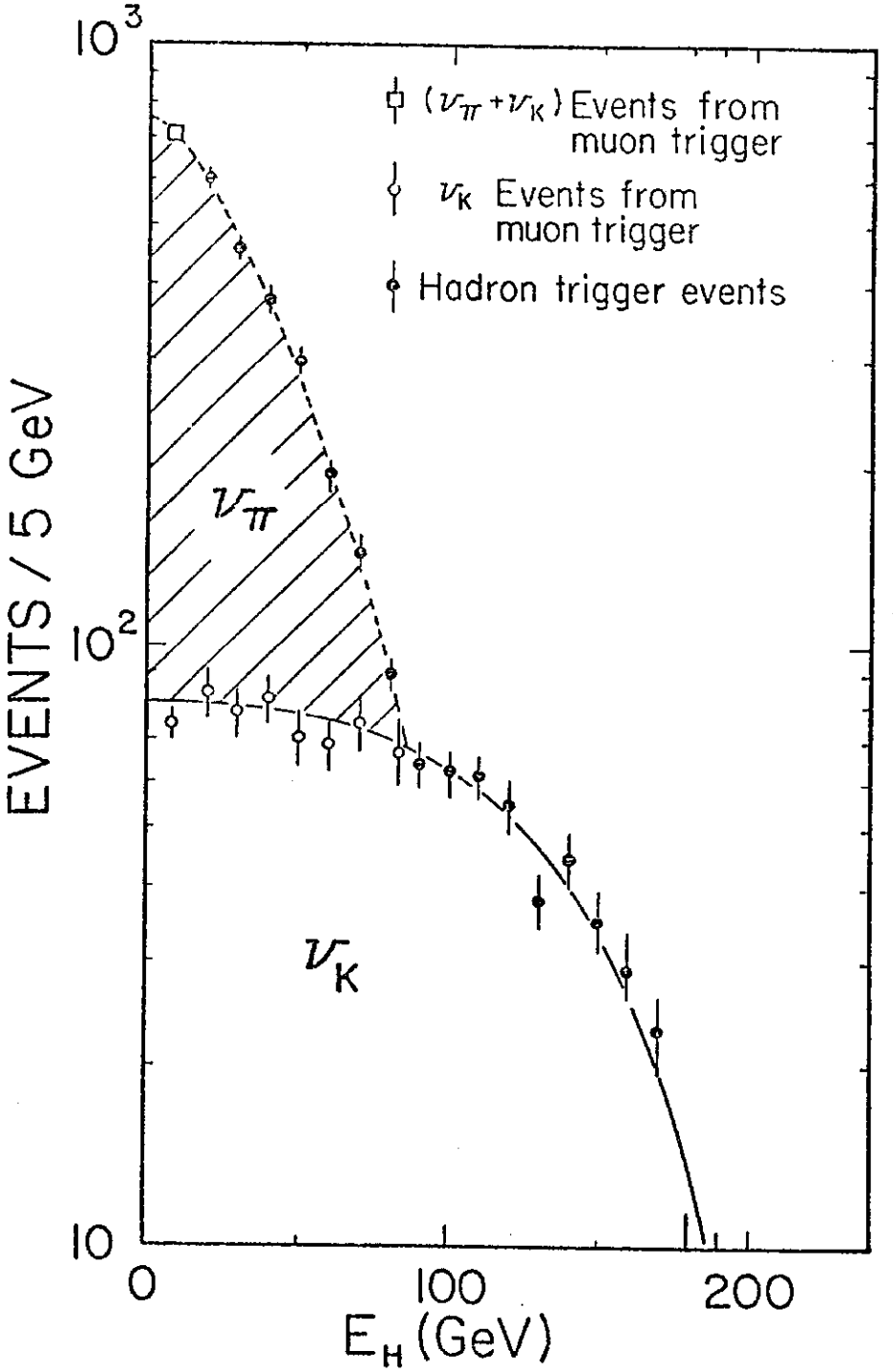

Fig. 9: Hadron energy histogram for all data at +190 GeV. Except for small corrections mentioned in the text this distribution is used to obtain both the number of events and the mean hadron energy for the ν_π and ν_K event samples.

hadron energy greater than E_{ν_π} can only result from ν_K. Figure 9 shows the hadron energy histogram for the +190 GeV running and demonstrates the separation of ν_K, ν_π data.

There is a small loss of data at large angles, or large y, due to the 360 mr acceptance cut. An estimate of the number of missing events is made by histogramming the scaled muon angle variable, $K_\theta \equiv 2M/E_\nu\theta^2$, which shows a small loss at low K_θ. Table II gives the estimated loss as a function of energy. The correction is less than 2% for antineutrinos and less than 7% for neutrinos.

Table II Estimated Event Loss Due to 360 mr Cut

E_ν (GeV)	Loss	$E_{\bar{\nu}}$ (GeV)	Loss
45.2	0.066±.021	45.9	0.016±.005
61.3	0.052±.015	60.6	0.000±.005
72.4	0.042±.013	65.7	0.013±.005
125.0	0.020±.007	129.0	0.00 ±.005
171.0	0.014±.005	168.0	0.00 ±.005
205.0	0.00 ±.005	188.0	0.00 ±.005

TOTAL CROSS SECTIONS

The values of the cross section and mean energies are given in Table III. They are shown graphically in Fig. 10. Included in the plot are the lower energy results from Gargamelle (GGM).[7,10] The GGM $\bar{\nu}$ slope of 0.28 goes through the $\bar{\nu}_\pi$ data but undershoots the $\bar{\nu}_K$ points. The ν slope of 0.74, which fits the GGM data well, is an overestimate for our high energy data. The best fit slopes, in units of σ/E are;

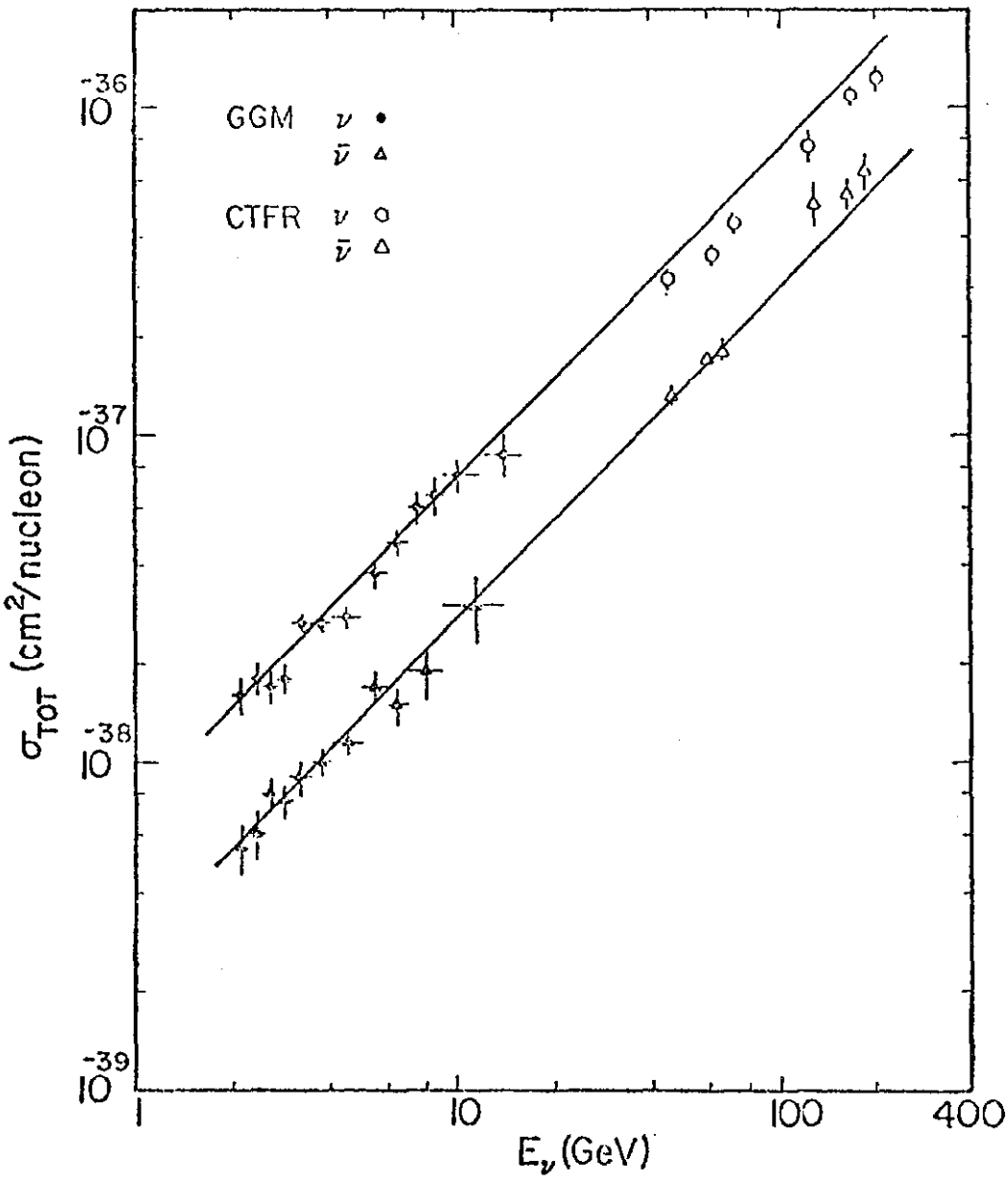

Fig. 10: Neutrino and antineutrino total cross sections. The lower energy results (E_ν < 12 GeV) from Gargamelle (GGM) are also shown. The curves are the GGM best fits at low energy extrapolated to the higher energy region of our measurements. See text for details.

$$S_\nu = 0.61 \pm 0.03 \times 10^{-38} \text{ cm}^2/\text{GeV},$$

$$S_{\bar{\nu}} = 0.29 \pm 0.015 \times 10^{-38} \text{ cm}^2/\text{GeV}$$

with χ^2 of 3.8 and 6.5, respectively, for 5 degrees of freedom. It is possible the decrease in the slope for neutrinos is consistent with scaling violations observed in ep and μp deep inelastic scattering. The cross sections reported here are in good agreement with BEBC data obtained in a recent CERN narrow band neutrino run.[11] The cross section ratio $\sigma_{\bar{\nu}}/\sigma_\nu$, of Fig. 11, shows a (20 ± 10)% rise from 45 GeV to the high energy points, 125 to 205 GeV. Our data do not show the more substantive rise reported by other authors.[2] This rise does not allow a right handed coupling quark (B quark) of mass 5-7 GeV which was suggested to explain the original measurements of HPWF.[12] It is possible to fit the cross section ratio with a combination of scaling violations and asymptotic freedom effects.[13]

Table III Cross Sections vs. Mean Neutrino Energy

E(GeV)	$\sigma^\nu (10^{-38}$ cm$^2)$	E(GeV)	$\sigma^{\bar{\nu}} (10^{-38}$ cm$^2)$
45.2	30.1±2.0	45.9	13.2±0.7
61.3	35.3±1.8	60.0	16.9±0.8
72.4	44.4±3.0	65.7	18.1±1.1
125.0	76.3±9.3	129.0	51.0±7.4
171.0	109.2±7.6	168.0	54.6±5.7
205.0	122.4±9.8	188.0	63.3±8.6

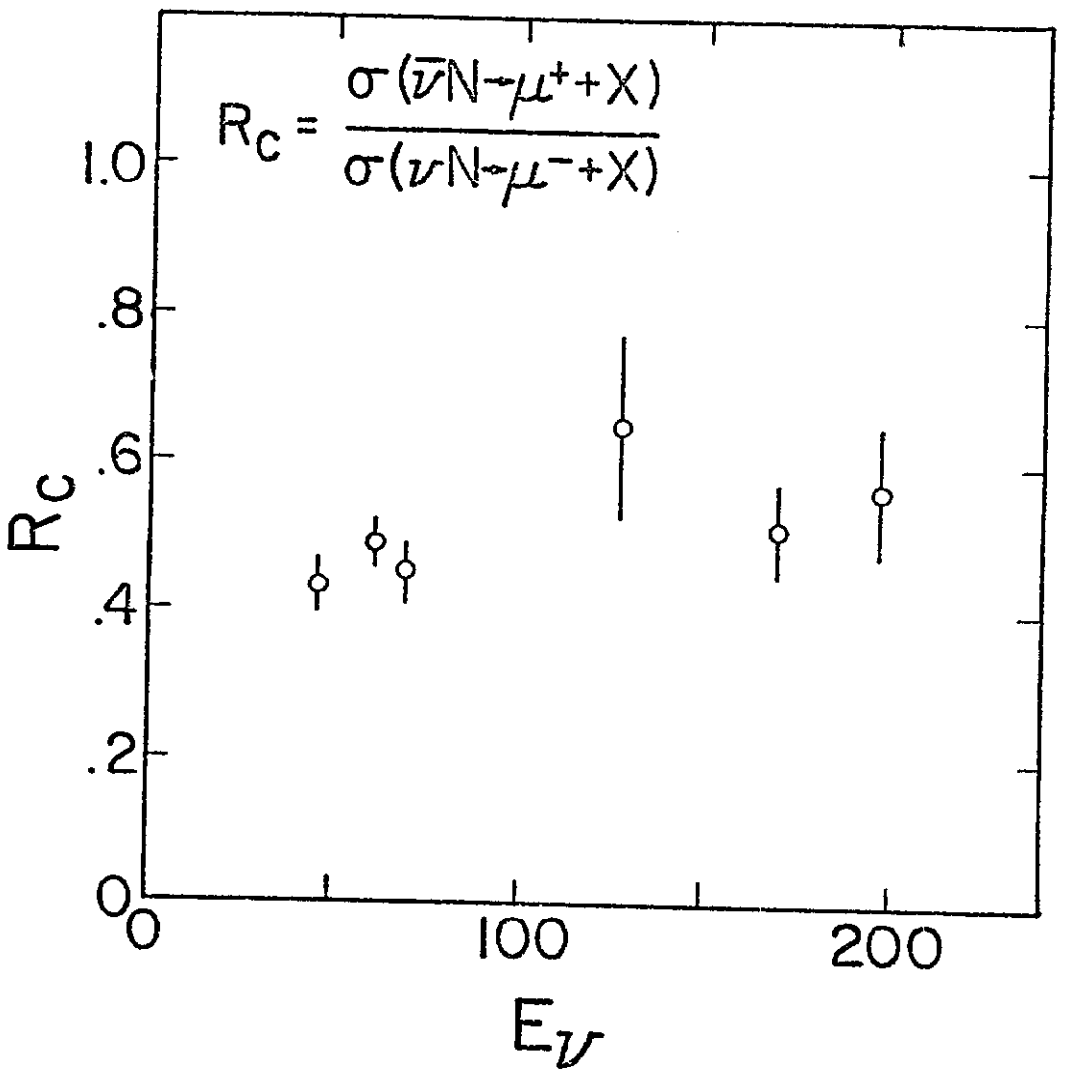

Fig. 11: Ratio of antineutrino and neutrino cross sections.

MEAN ELASTICITY

From the acceptance considerations discussed earlier it is clear the y distribution has missing events at high y because the muon energy is unmeasured. On the other hand the ν_K and ν_π hadron energy distribution is measured. Using our knowledge of the mean beam energy with position in the detector we can establish a mean neutrino energy which allows a calculation of $< y > = < E_H > / < E_\nu >$. The equivalence of $< E_H >$ with $< y > * < E_\nu >$ follows from the central limit theorem and integration of the hadron energy resolution function over a complete sample of data in our apparatus. A small correction to $< y >$ is necessary for the data which escapes both the muon and hadron trigger conditions ($\theta_\mu > 350$ mr). Figure 12 shows the $< y >$ versus neutrino energy and the values are given in Table IV. Again it is noted that we measure no unusually significant increase as was found by previous authors (the high y anomaly). Averaging over the six energies one finds $< y_\nu > = 0.47 \pm 0.01$ and $< y_{\bar{\nu}} > = 0.32 \pm 0.01$. These values are consistent with the BEBC data and our previously published data.[14] For the antineutrino data the 10% increase in $< y >$ from the lower energies (65 GeV) to the higher energies (150 GeV) may be related to the (20 ± 10)% increase in $\sigma_{\bar{\nu}}$ discussed earlier.

Table IV $< y >$ vs. Mean Neutrino Energy

E(GeV)	$< y >^{\nu}$	E(GeV)	$< y >^{\bar{\nu}}$
45.2	0.487±.026	45.9	.306 ± .014
61.3	0.461±.022	60.0	.314 ± .016
72.4	0.452±.023	65.7	.314 ± .016
125.0	0.503±.026	129.0	.343 ± .020
171.0	0.473±.020	168.0	.350 ± .022
205.0	0.476±.022	188.0	.339 ± .029

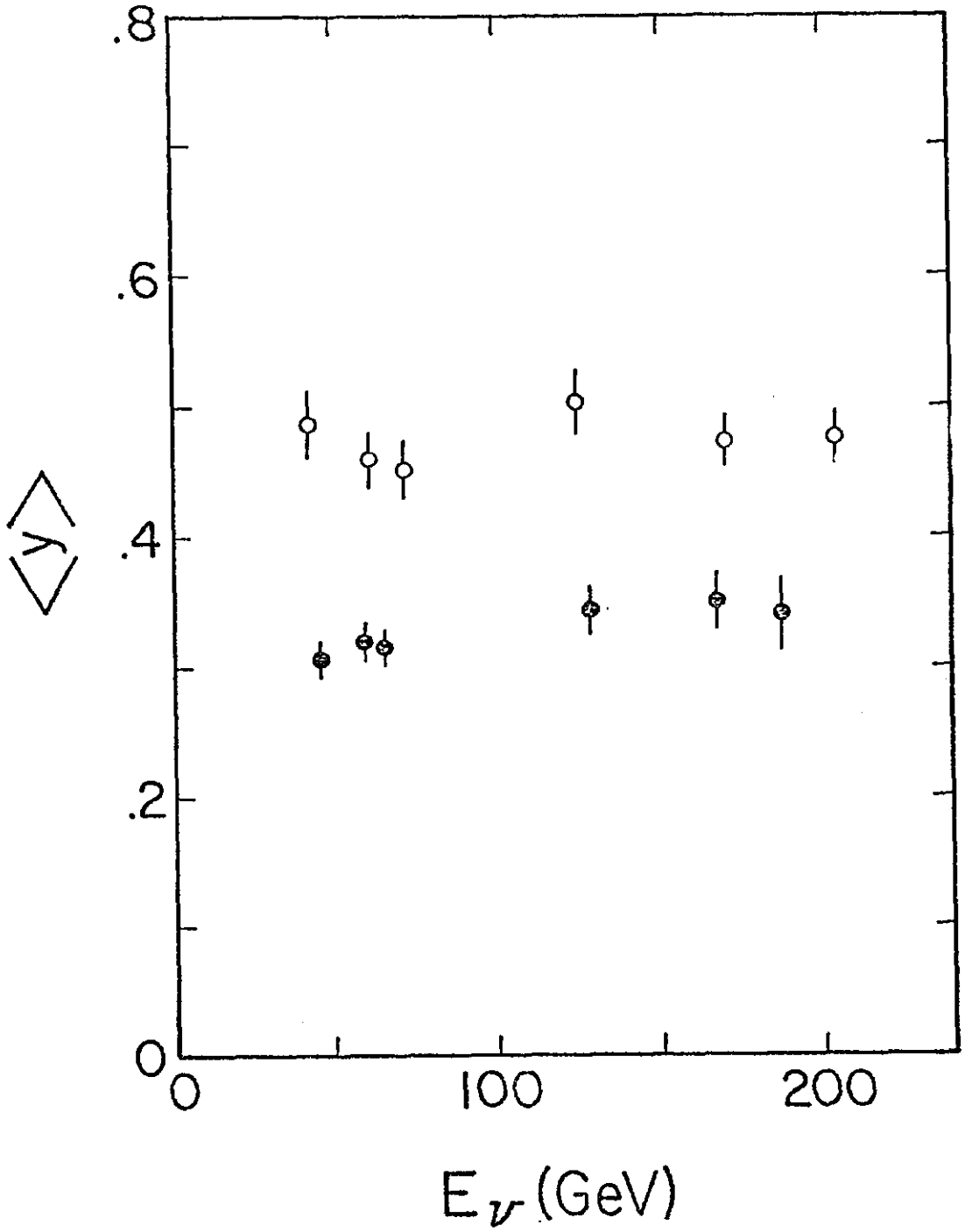

Fig. 12: Mean Inelasticity, < y >, for neutrinos (open circles) and antineutrinos (closed circles).

INTEGRATED STRUCTURE FUNCTIONS

Integration of Eq. (3) and calculation of the first moment of the y distribution yields:

$$\sigma^{\nu,\bar{\nu}} = \frac{G^2 ME}{\pi} \left\{\frac{1}{3} f_1 + \frac{1}{2} f_2 \pm \frac{1}{3} f_3\right\}, \qquad (4)$$

$$\sigma^{\nu,\bar{\nu}} < y >^{\nu,\bar{\nu}} = \frac{G^2 ME}{\pi} \left\{\frac{1}{4} f_1 + \frac{1}{6} f_2 \pm \frac{5}{24} f_3\right\}. \qquad (5)$$

Since there are three structure functions and four measured moments, the consistency of the structure functions can be tested. One way to see this is to define the ratios:

$$S_{\pm} = \frac{\sigma^{\nu} < y >^{\nu} \pm \sigma^{\bar{\nu}} < y >^{\bar{\nu}}}{\sigma^{\nu} \pm \sigma^{\bar{\nu}}} . \qquad (6)$$

The S_- ratio, displayed in Fig. 13 as a function of energy shows the consistency of the f_3 determination. The assumption of spin 1/2 for the partons (i.e., Callen-Gross, $2f_1 = f_2$) implies $S_+ = 7/16$ and the data of Fig. 13 are reasonably consistent with this value. If, however, one lets $\Delta \equiv (f_2 - 2f_1)/f_2$ then $S_+ = (7-3\Delta)/16-4\Delta)$. The measured mean of $S_+ = 0.424 \pm 0.007$ gives $= 0.17 \pm 0.09$ which implies a small violation of Callen-Gross at the two standard deviation level.

With the assumption, $2f_1 = f_2$, the integrated structure functions, f_2 and f_3, have been fitted to the zeroth and first moments of the y distributions. These are displayed in Fig. 14 where it is evident there is a gradual decrease in the value of f_3 with energy. This effect which may be associated with scale breaking or other phenomena is equivalently seen as a decrease in the B parameter ($B \equiv f_3/f_2$) or as an increase in the fractional amount of momentum carried by the antiquark in the nucleon as $E_{\nu,\bar{\nu}}$ is increased.

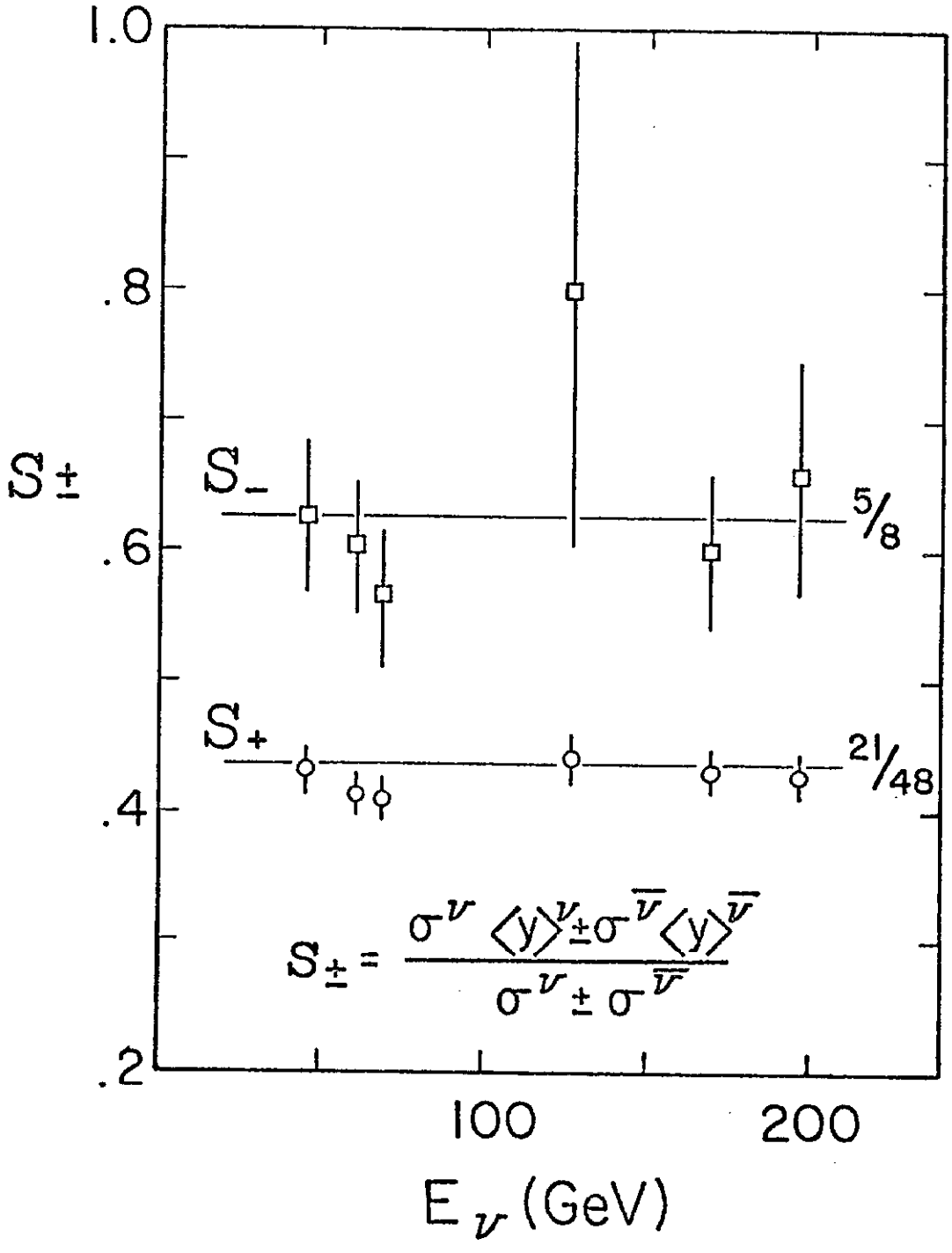

Fig. 13: Integrated structure function ratios.

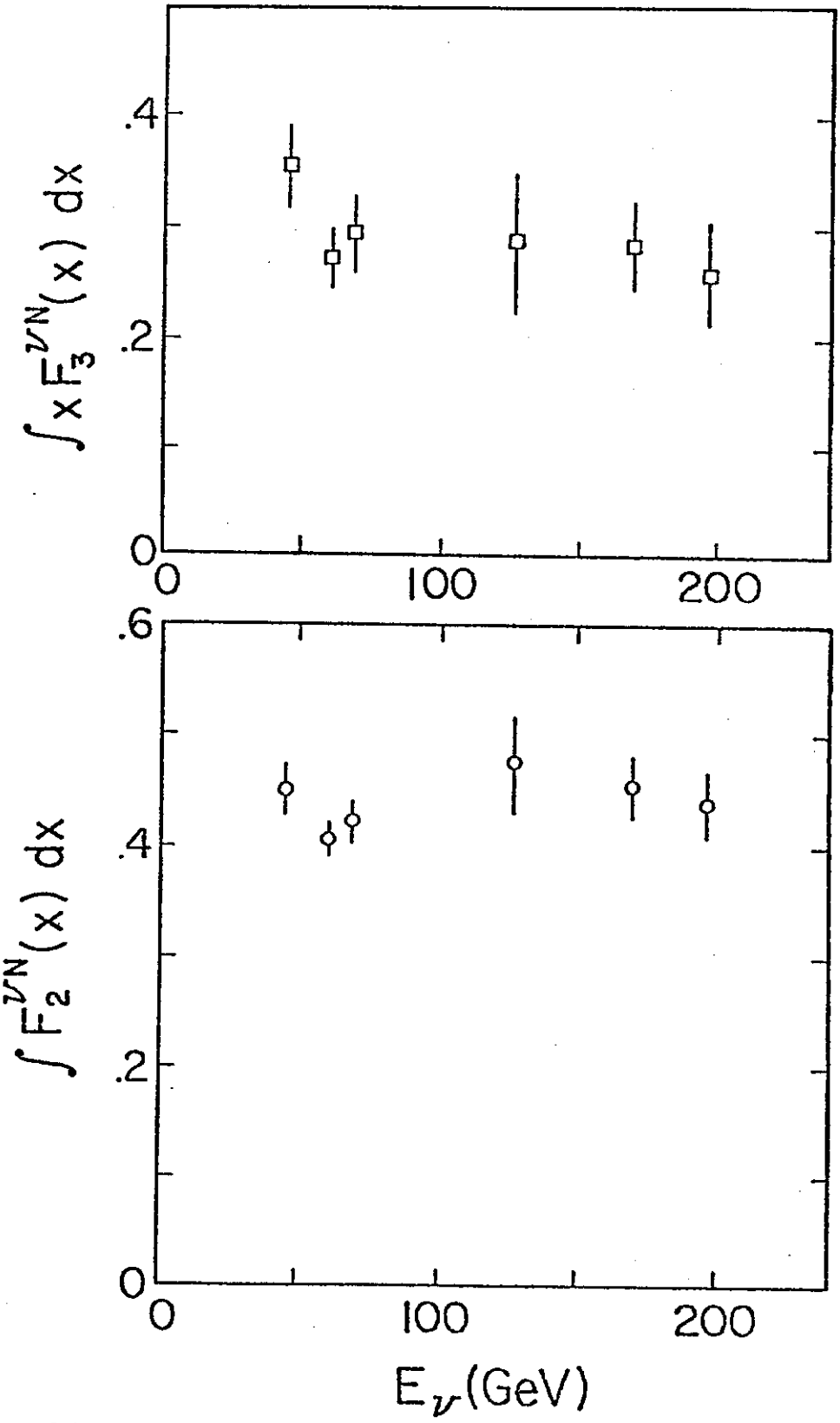

Fig. 14: Integrated structure functions.

CONCLUSIONS

(1) Charge symmetry invariance, as measured by comparing the equivalence of neutrino and antineutrino cross sections at $y = 0$, is valid to about 5%. The value of f_2 obtained at low y is consistent with predictions which relate charged lepton and neutrino deep-inelastic scattering.

(2) The mean y and σ^{ν}/E, for neutrinos, is flat from $45 \leq E_{\nu} \leq 205$ GeV. The value of $\sigma^{\nu}/E = 0.61$ is less than the lower energy value 0.74 of Gargamelle.

(3) For antineutrinos $\sigma^{\bar{\nu}}/E$ shows a (20 ± 10)% rise above 100 GeV and $< y >$ increases (10 ± 5)% in the same energy region. σ^{ν}/E for energies less than 100 GeV is consistent with the Gargamelle value of 0.28.

(4) Right-handed quarks, coupled full strength via the weak coupling constant to u quarks, are ruled out for masses less than 8 GeV.

(5) There is evidence for scale breaking, especially in f_3 and some indication at the two standard deviation[3] level, for a small violation of the Callen-Gross relation.

REFERENCES

(a) Present address: Fermi National Accelerator Laboratory, Batavia, Illinois 60510.
(b) Present address: University of Rochester, Rochester, New York 14627.
(c) Present address: Northwestern University, Evanston, Illinois 60201.

1. C. H. Llewellyn-Smith, Physics Reports 36, 263 (1972).
2. A. Benvenuti et al., Phys. Rev. Lett. 37, 189 (1976).
3. A. Benvenuti et al., Phys. Rev. Lett. 36, 1478 (1976).
4. M. Holder et al., Phys. Rev. Lett. 39, 433 (1977).
5. P. Limon et al., Nucl. Instrum. Methods 116, 317 (1974).
6. B. C. Barish et al., Phys. Rev. Lett. 35, 1316 (1975).
   B. C. Barish et al., Nucl. Instrum. Methods 130, 49 (1975).
7. D. H. Perkins, Reports on Progress in Physics 40, 409 (1977).
8. H. L. Anderson et al., Phys. Rev. Lett. 37, 4 (1976).
9. J. I. Friedman and H. W. Kendall, Annual Review of Nucl. Sci. 22, 203 (1972).
10. T. Eichten et al., Phys. Lett. 46B, 281 (1973).
11. P. C. Bosetti et al., Phys. Lett. 70B, 273 (1977).
12. R. M. Barnett, Phys. Rev. Lett. 36, 1163 (1976) and R. M. Barnett, H. Georgi, and H. D. Politzer, Phys. Rev. Lett. 37, 1313 (1976).
13. F. J. Sciulli, Private Communication. See e.g., I. Hinchliffe and C. H. Llewellyn Smith, Phys. Lett. 70B, 247 (1977).
14. B. C. Barish et al., Phys. Rev. Lett. 38, 314 (1977).